East European Journal of Physics. 2. 405-411 (2025)
DOI:10.26565/2312-4334-2025-2-49 ISSN 2312-4334

IN SILICO CHARACTERIZATION OF TECHNETIUM-99M RADIOTRACERS: ADMET PROPERTIES AND PROTEIN INTERACTION PROFILES

V. Trusova[a]*, U. Malovytsia[a], P. Kuznietsov[b], I. Yakymenko[b], G. Gorbenko[a]
[a]*Department of Medical Physics and Biomedical Nanotechnologies, V.N. Karazin Kharkiv National University 4 Svobody Sq., Kharkiv, 61022, Ukraine*
[b]*O.I. Akhiezer Department for Nuclear Physics and High Energy Physics, V.N. Karazin Kharkiv National University 4 Svobody Sq., Kharkiv, 61022, Ukraine*
**Corresponding Author: valerija.trusova@karazin.ua*
Received February 28, 2025, revised March 17, 2025; accepted April 30, 2025

The rational design of technetium-99m (^{99m}Tc)-based radiopharmaceuticals requires a nuanced understanding of how physicochemical properties influence *in vivo* behavior and molecular interactions. In this study, we employed an integrated *in silico* framework to characterize ten clinically relevant ^{99m}Tc-labeled tracers using ADMET prediction, molecular docking with functional proteins (albumin, insulin, lysozyme), and multivariate statistical analysis. The results revealed that polarity, hydrogen bonding capacity, and molecular flexibility critically govern both pharmacokinetic properties and protein-binding profiles. Tracers such as TcSES and TcTET, with low topological polar surface area and minimal binding affinity, were associated with rapid clearance and are well suited for dynamic imaging protocols. In contrast, compounds like TcDTPA and TcDIS demonstrated strong albumin interaction and metabolic stability, supporting their use in delayed-phase imaging. TcHYN emerged as a unique tracer, exhibiting extreme polarity and promiscuous high-affinity binding across multiple protein targets. Principal component analysis and hierarchical clustering grouped tracers into functionally distinct categories, highlighting structure-dependent design trends. Collectively, these findings suggest that combined ADMET-docking profiling offers a scalable strategy for preclinical evaluation and supports the development of safer, more targeted ^{99m}Tc-based radiopharmaceuticals.
Keywords: *Technetium-based radiotracers; Human serum albumin; Lysozyme; Insulin; Molecular docking; SPECT imaging*
PACS: 87.14.C++c, 87.16.Dg

Radiotracers based on technetium-99m (^{99m}Tc) remain at the forefront of diagnostic nuclear medicine, enabling non-invasive visualization of physiological and pathological processes across a broad spectrum of clinical applications [1]. Their widespread use is underpinned by favorable nuclear properties, well-established radiochemistry, and ability to tailor molecular structures for targeted imaging of specific organs and disease states. However, the continual evolution of molecular imaging demands rigorous preclinical evaluation of new and existing radiotracers to optimize their pharmacokinetic behavior, safety, and diagnostic efficacy. Along with high target specificity, the effective design of radiopharmaceuticals necessitates optimal biodistribution, metabolic stability, minimal off-target toxicity, and favorable protein-binding characteristics. In particular, interactions with transport and carrier proteins, such as serum albumin, insulin, and lysozyme, can profoundly influence plasma retention, tissue delivery, and imaging contrast [2]. However, systematic molecular-level comparisons across multiple ^{99m}Tc compounds are rarely undertaken, in part due to the cost and complexity of experimental pharmacological profiling. In this context, *in silico* methodologies offer a compelling alternative. In particular, advanced platforms such as ADMETlab 3.0 enable high-throughput prediction of absorption, distribution, metabolism, excretion, and toxicity (ADMET) properties [3], while molecular docking allows for detailed interrogation of tracer-protein interactions at atomic resolution. When used in concert, these tools provide a multidimensional framework for evaluating the safety, efficacy, and mechanistic underpinnings of radiopharmaceuticals. The present work is directed at comprehensive *in silico* characterization of clinically relevant ^{99m}Tc-based tracers, integrating ADMET predictions with molecular docking against three functionally relevant proteins, human serum albumin, insulin, and lysozyme. Our aim is to uncover structure-dependent trends in pharmacokinetics and binding profiles, offering mechanistic insights that may guide future tracer design and optimization strategies.

METHODS

A representative set of ten clinically utilized technetium-99m (^{99m}Tc)-based radiopharmaceuticals was selected to capture structural diversity across approved diagnostic agents. The compounds analyzed included [^{99m}Tc]Tc-Sestamibi (TcSES), [^{99m}Tc]Tc-Tetrofosmin (TcTET), [^{99m}Tc]Tc-Medronate (TcMED), [^{99m}Tc]Tc-dimercaptosuccinic acid (TcDMSA), [^{99m}Tc]Tc-diethylenetriaminepentaacetate (TcDTPA), [^{99m}Tc]Tc-mercaptoacetyltriglycine (TcMAG), [^{99m}Tc]Tc-diisopropyl iminodiacetic acid (TcDIS), [^{99m}Tc]Tc-ethylene cysteine dimer (TcECD), [^{99m}Tc]Tc-Mebrofenin (TcMEB), and [^{99m}Tc]Tc-hydrazinonicotinic acid conjugate-H6F (TcHYN). Physicochemical and pharmacokinetic parameters were predicted using ADMETlab 3.0 (https://admetlab3.scbdd.com/), an integrated platform for the data-driven prediction of ADME and toxicity profiles. Each compound was converted to a canonical SMILES representation

Cite as: V. Trusova, U. Malovytsia, P. Kuznietsov, I. Yakymenko, G. Gorbenko, East Eur. J. Phys. 2, 405 (2025), https://doi.org/10.26565/2312-4334-2025-2-49

and processed through the platform to retrieve a comprehensive panel of descriptors. Predicted parameters included molecular weight, topological polar surface area (TPSA), partition coefficient (logP), hydrogen bond donors and acceptors, number of rotatable bonds, and absorption-related features such as human intestinal absorption (HIA) and Caco-2 permeability. Additional metrics included plasma protein binding (PPB), volume of distribution (VDss), blood-brain barrier (BBB) penetration, hepatic microsomal stability (HLM), total plasma clearance (CL), and biological half-life ($T_{1/2}$). Toxicity endpoints, including AMES mutagenicity, hERG inhibition, drug-induced liver injury (DILI), skin sensitization, and carcinogenicity, were also assessed. Three biologically relevant proteins, human serum albumin (PDB ID 1AO6), human insulin (PDB ID 4EYN), and human lysozyme (PDB ID 8Y9W), were selected as docking targets to evaluate potential interactions of ^{99m}Tc-tracers with endogenous carrier and regulatory proteins. Prior to docking, each protein structure was subjected to 10 ns molecular dynamics relaxation using a standard explicit solvent protocol to ensure conformational stabilization. Relaxation simulations were performed with position restraints applied to backbone atoms and standard temperature and pressure conditions. Molecular docking simulations were performed using the HDOCK server (https://hdock.phys.hust.edu.cn/) [4], a hybrid docking platform integrating template-based modeling and free docking via a fast FFT-based algorithm. All ligands were submitted as energy-minimized structures. For each protein-ligand pair, blind docking was conducted to explore global interaction surfaces.

RESULTS AND DISCUSSION

Due to the diversity of their chelating ligands and pharmacophore groups, TCC exhibit substantial chemical heterogeneity. This complexity underlies their varying pharmacokinetics, biodistribution, and safety profiles. To systematize this variability, we conducted a high-throughput computational analysis of ten clinically employed ^{99m}Tc-labeled compounds using the ADMETlab 3.0 platform, focusing on key descriptors of absorption, distribution, metabolism, excretion, and toxicity (ADMET). The results are given in Table 1.

Table 1. ADMET properties of ^{99m}Tc-based radiopharmaceuticals

		TcSES	**TcTET**	**TcMED**	**TcDMSA**	**TcDTPA**	**TcMAG**	**TcDIS**	**TcECD**	**TcMEB**	**TcHYN**
Physicochemical properties	Molecular weight	113.08	382.24	173.95	181.97	393.14	259.03	350.18	321.1	386.05	1252.6
	TPSA	13.59	36.92	120.72	74.6	196.22	133.64	106.94	78.73	106.94	438.63
	logP	1.084	2.179	-2.092	0.4	-0.914	0.34	0.055	1.561	-0.003	1.334
	Number of hydrogen bond acceptors	2	4	6	4	13	8	7	6	7	27
	Number of hydrogen bond donors	0	0	2	2	5	0	3	1	3	16
	Number of rotatable bonds	2	19	2	3	16	10	10	13	8	45
Absorption	HIA	0.018	0.028	0.964	0.317	1	0.016	0.798	0.009	0.445	0.606
	Caco-2 permeability	-4.727	-5.189	-5.94	-4.884	-5.195	-4.821	-5.16	-5.542	-5.305	-6.215
	P-gp substrate	0.063	0.094	0	0.002	0	0.001	0	0	0	0.003
Distribution	VDss	0.115	0.028	-0.26	-0.171	-0.54	-0.413	-0.278	0.199	0.075	-0.578
	BBB permeability	0.285	0.096	0	0.001	0	0.216	0	0	0	0
	PPB	27.95	12.97	12.224	94.613	14.538	7.819	92.556	57.144	97.438	77.494
Metabolism	CYP2D6 inhibitor	0	0.38	0	0	0	0	0	0	0	0
	CYP3A4 inhibitor	0	0.408	0	0	0	0	0	0.59	0	0
	HLM stability	0	0.755	0.003	0.286	0.077	0.002	0.953	0.989	0.21	0
Excretion	CL_{plasma}	10.213	8.257	1.518	1.953	1.464	2.021	2.346	5.701	2.088	0.844
	$T_{1/2}$	1.739	0.797	2.224	1.97	1.528	1.801	1.158	0.784	1.264	1.563
Toxicity	AMES	1	0.023	0.078	0.332	0.514	0.782	0.149	0.935	0.172	0.046
	hERG	1	0.728	0.269	0.181	0.033	0.013	0.165	0.004	0.093	0.052
	DILI	0.116	0.006	0.467	0.974	0.331	0.779	0.142	1	0.222	0.91
	Skin sensitization	1	0.991	0.997	0.857	0.774	1	0.951	1	0.98	0.557
	Carcinogenicity	1	0.409	0.987	0.009	0.138	0.196	0.853	0.032	0.883	0.574

As seen from this table, the examined TCC are characterized by a broad distribution in molecular weight (113.08-1252.6 Da), topological polar surface area (TPSA 13.59-438.63 Å^2), and lipophilicity (logP; from -2.092 to 2.179). As expected, two cationic, lipophilic agents used for myocardial perfusion imaging, TcSES and TcTET, exhibited low polarity (TPSA < 40 Å^2), moderate lipophilicity, and minimal hydrogen bonding potential. These values align closely with their

experimentally established passive membrane permeability and mitochondrial accumulation [5]. In contrast, highly polar tracers such as TcDTPA and TcHYNIC demonstrated elevated TPSA and rotatable bond counts, aligning with their renal clearance and low membrane permeability [6]. Predicted absorption characteristics were found to correlate also with the reported clinical behavior of TCC. High human intestinal absorption (HIA > 0.75) was observed for TcDIS and TcMED, the tracers previously evaluated for enteral administration under experimental protocols. In contrast, TCC with reduced HIA and Caco-2 permeability (e.g., TcHYNIC, TcDTPA) are administered strictly via intravenous routes, consistent with their poor predicted epithelial transport.

Analysis of the systemic distribution revealed general low tissue accumulation, as can be judged from the values of VDss which are ranged from -0.578 to 0.199 L/kg. Notably, only TcSES and TcMAG exhibited predicted blood-brain barrier (BBB) penetration probabilities above the threshold of 0.2, being in partial agreement with prior studies reporting minimal but detectable cerebral uptake for lipophilic cationic complexes. Predicted plasma protein binding (PPB) was also dependent in TCC chemical structure. Specifically, TcMEB, TcDIS and TcDMSA showed PPB > 90%, which is in line with empirical data confirming strong affinity to serum albumin [7], whereas TcMAG and TcTET exhibited lower predicted values (<15%), suggesting more rapid plasma clearance.

Predicted hepatic microsomal stability (HLM) also varied markedly across tracers. TcDIS and TcECD exhibited high metabolic stability (HLM > 0.95), consistent with renal excretion, whereas TcSES and TcMAG showed minimal stability, aligning with their known hepatobiliary clearance [8,9]. These metabolic trends were reflected in plasma clearance values, with TcSES demonstrating the highest systemic turnover (10.2 mL/min/kg). All compounds exhibited half-lives within the clinically favorable range (0.78-2.22 h), balancing imaging efficiency and radiation safety. TcTET and TcECD showed the shortest predicted half-lives, supporting their utility in dynamic protocols. Toxicity predictions revealed elevated hERG inhibition risk for TcSES and TcTET, likely due to their cationic lipophilicity and mitochondrial affinity. TcECD and TcHYNIC were associated with high DILI risk, while TcMED and TcMEB showed increased carcinogenicity potential. These findings warrant further *in vivo* validation, particularly for tracers considered for repeated or high-dose use.

To explore molecular determinants of tracer-protein interactions, we next conducted docking simulations against human serum albumin (HSA), lysozyme (HLz), and insulin (HIns). The best scored docking poses of the protein-TCC complexes are presented in Fig. 1.

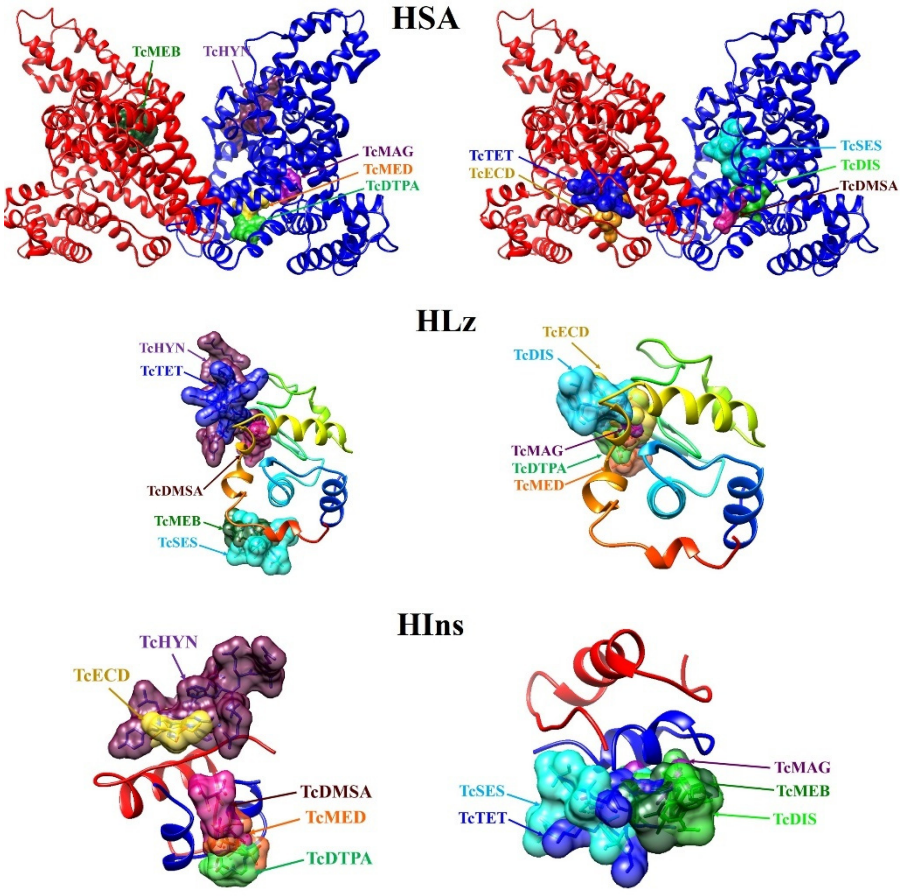

Figure 1. Best docking poses of the protein-TCC complexes

The resulting interaction scores and interface maps revealed compound-specific trends in affinity, interaction types, and binding site architecture (Tables 2-5). The analysis of the obtained data revealed marked differences in binding

affinity, interaction type, and binding site localization. Accordingly, TcHYN exhibited the strongest affinity across all targets (-249.5 for HSA, -194.8 for HLz, and -163.7 for HIns), driven by its extended π-system, high polar surface area, and flexible coordination geometry. TcDTPA and TcDIS also showed strong binding, particularly to albumin, reflecting their polyanionic nature and multivalent hydrogen bonding. In contrast, TcSES and TcTET displayed weaker binding, particularly to insulin, suggesting passive diffusion may be their dominant transport mechanism.

Table 2. Binding affinities of technetium-99m radiopharmaceuticals for functional proteins

TCC	Albumin	Lysozyme	Insulin
TcSES	-148.84	-138.37	-116.92
TcTET	-141.24	-126.06	-121.66
TcMED	-137.01	-133.67	-96.81
TcMAG	-137.33	-127.38	-105.69
TcECD	-137.71	-120.27	-99.43
TcDMSA	-156.73	-132.46	-100.25
TcDIS	-170.32	-162.07	-143.44
TcDTPA	-182.8	-149.79	-129.09
TcHYN	-249.51	-194.79	-163.74
TcMEB	-159.93	-153.45	-137.67

Table 3. Interface residues in the complexes of technetium-99m radiopharmaceuticals with human serum albumin

TCC	**HSA-TCC interface residues**	**Type of interactions**
TcSES	TYR_{150A}, GLU_{153A}, PHE_{156A}, PHE_{157A}, ARG_{160A}, GLU_{188A}, ALA_{191A}, SER_{192A}, LYS_{195A}, GLN_{196A}, LYS_{199A}, ARG_{218A}, ARG_{222A}, HSD_{288A}, GLU_{292A}, VAL_{293A}, LYS_{436A}, HSD_{440A}, TYR_{452A}	Hydrophobic interactions, hydrogen bonds
TcTET	ASN_{109B}, ARG_{114B}, LEU_{115B}, ARG_{145B}, LYS_{190B}, GLU_{425B}, ARG_{428B}, GLU_{520B}, ILE_{523B}	Hydrophobic interactions, hydrogen bonds
TcMED	LEU_{115A}, ARG_{117A}, TYR_{138A}, ILE_{142A}, HSD_{146A}, PHE_{149A}, LEU_{154A}, PHE_{157A}, TYR_{161A}, LEU_{182A}, ASP_{183A}, LEU_{185A}, ARG_{186A}, ASP_{187A}, GLY_{189A}, LYS_{190A}	Hydrogen bonds
TcMAG	ASP_{107A}, ASP_{108A}, ASN_{109A}, ARG_{145A}, HSD_{146A}, PRO_{147A}, TYR_{148A}, LYS_{190A}, ALA_{191A}, SER_{193A}, ALA_{194A}, ARG_{197A}, GLU_{425A}, ASN_{458A}, GLN_{459A}	Hydrogen bonds, salt bridges
TcECD	LEU_{115B}, ARG_{117B}, PRO_{118B}, MET_{123B}, PHE_{134B}, LYS_{137B}, TYR_{138B}, GLU_{141B}, ILE_{142B}, TYR_{161B}, LEU_{182B}, ASP_{183B}, LEU_{185B}, ARG_{186B}	Hydrophobic interactions, hydrogen bonds, salt bridges
TcDMSA	LEU_{115A}, VAL_{116A}, ARG_{117A}, PRO_{118A}, MET_{123A}, TYR_{138A}, ILE_{142A}, HSD_{146A}, PHE_{149A}, LEU_{154A}, PHE_{157A}, TYR_{161A}, LEU_{182A}, LEU_{185A}, ARG_{186A}, ASP_{187A}, GLU_{188A}, GLY_{189A}, LYS_{190A}	Hydrogen bonds, salt bridges
TcDIS	ASN_{109A}, PRO_{110A}, LEU_{112A}, ARG_{114A}, LEU_{115A}, ARG_{145A}, HSD_{146A}, ARG_{186A}, LYS_{190A}, PRO_{421A}, GLU_{425A}, GLU_{520A}, ILE_{523A}	Hydrophobic interactions, hydrogen bonds
TcDTPA	LEU_{115A}, VAL_{116A}, ARG_{117A}, PRO_{118A}, MET_{123A}, PHE_{134A}, LEU_{135A}, LYS_{137A}, TYR_{138A}, GLU_{141A}, ILE_{142A}, TYR_{161A}, LEU_{182A}, ARG_{186A}	Hydrogen bonds, salt bridges
TcHYN	GLU_{383A}, LEU_{387A}, ASN_{391A}, LEU_{394A}, LEU_{407A}, VAL_{409A}, ARG_{410A}, TYR_{411A}, LEU_{430A}, LEU_{453A}, GLU_{492A}, SER_{489A}, LYS_{541A}, GLU_{542A}, LYS_{545A}	Hydrogen bonds, π-stacking, salt bridges
TcMEB	GLU_{188B}, LYS_{195B}, TRP_{214B}, ARG_{218B}, GLN_{221B}, ARG_{222B}, GLU_{292B}, VAL_{293B}, GLU_{294B}, ASN_{295B}, LYS_{436B}, HSD_{440B}, LYS_{444B}, PRO_{447B}, CYS_{448B}, ALA_{449B}, ASP_{451B}, TYR_{452B}	Hydrophobic interactions, hydrogen bonds, salt bridges

Table 4. Interface residues in the complexes of technetium-99m radiopharmaceuticals with human lysozyme

TCC	**HLz-TCC interface residues**	**Type of interactions**
TcSES	ARG_5 CYS_{30} LYS_{33} TRP_{34} TYR_{38} ARG_{115} CYS_{116} ARG_{119} ASP_{120} VAL_{121} ARG_{122} GLN_{123} TYR_{124}	Hydrogen bonds, hydrophobic interactions
TcTET	TYR_{63}, VAL_{74}, ASN_{75}, ARG_{107}	Hydrophobic interactions
TcMED	GLU_{35} ASN_{44} ASN_{46} SER_{51} ASP_{53} GLN_{58} ILE_{59} ASN_{60} ALA_{108} TRP_{109} VAL_{110} ALA_{111}	Hydrogen bonds
TcMAG	GLU_{35} ASN_{46} ASP_{49} SER_{51} ASP_{53} GLN_{58} ILE_{59} ASN_{60} ARG_{62} TYR_{63} TRP_{64} ALA_{108} TRP_{109}	Hydrogen bonds
TcECD	GLU_{35} ASN_{44} ASN_{46} ASP_{49} ASP_{53} GLN_{58} ILE_{59} ASN_{60} SER_{61} ARG_{62} TYR_{63} TRP_{64} VAL_{99} GLY_{105} ALA_{108} TRP_{109} VAL_{110}	Hydrogen bonds

TCC	HLz-TCC interface residues	Type of interactions
TcDMSA	GLU_{35} ASN_{44} ASN_{46} ASP_{53} GLN_{58} ILE_{59} ASN_{60} SER_{61} ARG_{62} TYR_{63} TRP_{64} VAL_{99} GLY_{105} ALA_{108} TRP_{109} VAL_{110} ALA_{111}	Hydrogen bonds
TcDIS	ASP_{49}, SER_{51}, ASN_{60}, ARG_{62}, TYR63, ASN_{75}, GLY_{105}, ALA_{108}	Hydrogen bonds, hydrophobic interactions
TcDTPA	GLU_{35} ASN_{44} ASN_{46} ASP_{49} SER_{51} ASP_{53} PHE_{57} GLN_{58} ILE_{59} ASN_{60} ARG_{62} TYR_{63} TRP_{64} ALA_{108} TRP_{109} VAL_{110} ALA_{111}	Hydrogen bonds
TcHYN	TYR_{1}, TYR_{63}, ASN_{75}	Hydrogen bonds, hydrophobic interactions, π-stacking
TcMEB	LYS_{33} TRP_{34} ASN_{114} ARG_{115} ARG_{119} ASP_{120} VAL_{121} ARG_{122} GLN_{123} TYR_{124}	Hydrophobic interactions, hydrogen bonds, salt bridges

Table 5. Interface residues in the complexes of technetium-99m radiopharmaceuticals with human insulin

TCC	HIns-TCC interface residues	Type of interactions
TcSES	GLY_{1A} ILE_{2A} GLN_{5A} TYR_{14A} GLN_{15A} ASN_{18A} TYR_{19A} CYS_{20A} ASN_{21A} PHE_{24B} PHE_{25B}	Hydrophobic interactions, hydrogen bonds
TcTET	GLN_{5A}, TYR_{14A}, ASN_{18A}, CYS_{7B}, GLU_{13B}, ALA_{14B}	Hydrophobic interactions, hydrogen bonds
TcMED	ILE_{2A} GLN_{5A} CYS_{6A} SER_{9A} ILE_{10A} TYR_{14A} GLN_{15A} ASN_{18A} TYR_{19A}	Hydrogen bonds
TcMAG	GLN_{5A} SER_{9A} ILE_{10A} CYS_{11A} SER_{12A} TYR_{14A} GLN_{15A} ASN_{18A} TYR_{19A}	Hydrogen bonds
TcECD	SER_{9B} $VAL1_{2B}$ TYR_{16B} PHE_{24B} PHE_{25B} TYR_{26B}	Hydrophobic interactions, hydrogen bonds
TcDMSA	ILE_{2A} GLN_{5A} TYR_{14A} GLN_{15A} ASN_{18A} TYR_{19A} CYS_{20A} ASN_{21A} PHE_{25B}	Hydrogen bonds
TcDIS	GLN_{5A}, SER_{9A}, SER_{12A}, TYR_{14A}, GLN_{15A}, ASN_{18A}, TYR_{19A}, CYS_{7B}, GLU_{13B}, ALA_{14B}	Hydrophobic interactions, hydrogen bonds
TcDTPA	GLN_{5A} CYS_{6A} SER_{9A} ILE_{10A} CYS_{11A} SER_{12A} TYR_{14A} GLN_{15A} ASN_{18A} TYR_{19A}	Hydrogen bonds
TcHYN	TYR_{1A}, CYS_{7B}, GLU_{13B}, ALA_{14B}, TYR_{26B}, THR_{27B}	Hydrogen bonds, hydrophobic interactions, π-stacking
TcMEB	GLU_{4A} GLN_{5A} CYS_{6A} THR_{8A} SER_{9A} ILE_{10A} CYS_{11A} SER_{12A} TYR_{14A} GLN_{15A} ASN_{18A} TYR_{19A}	Hydrophobic interactions, hydrogen bonds

All TCC were characterized by different binding sites within the protein molecules. Specifically, TcHYN was shown to bind to HSA in the Sudlow site II [10] via TYR_{411A} and ARG_{410A} through hydrogen bonding and π-stacking. TcDIS engaged the GLU_{520A}–ILE_{523A} region through hydrophobic and hydrogen bonds contacts. In turn, TcMEB was found to be localized within the chain B of the protein (residues ARG_{218B}–ARG_{222B}, LYS_{436B}–TYR_{452B}), consistent with its known *in vivo* albumin affinity and prolonged circulation. Such interactions are beneficial for stabilizing tracers in the bloodstream and facilitating organ-specific targeting.

Lysozyme binding followed a conserved pattern across high-affinity tracers, with GLU35, $ASN_{44\text{-}60}$, and TYR_{63} commonly involved in hydrogen bonding. TcHYN displayed additional π–π stacking interactions with TYR63 and formed hydrophobic contacts with ASN_{75}, further stabilizing the complex. These interactions appear to be driven by shape complementarity and the presence of polar and aromatic functional groups on the tracer surface, rather than by strong site-specific recognition.

Insulin presented a more selective interaction interface compared to transport proteins, with docking localized to structurally and functionally relevant surface regions. TcHYN and TcDIS demonstrated the highest binding affinities, forming interactions with residues located on the B-chain surface, though not directly with core receptor-binding residues such as PHE_{24B}. Some tracers, including TcSES and TcDMSA, formed hydrogen bonds with TYR_{14A} and GLN_{15A} of the A-chain, situated near the receptor-binding groove. While the low concentrations of radiotracers used in SPECT imaging are unlikely to perturb insulin function, the engagement of tracers with surface-accessible residues adjacent to biologically critical domains reinforces the need for careful evaluation of biochemical neutrality, particularly in the context of metabolic disorders.

To emerge the above findings into a predictive framework, we applied principal component analysis and hierarchical clustering to the combined ADMET and docking dataset. The resulting PCA plot (Fig. 2, left panel) revealed a structured spatial distribution of tracers, with distinct segregation according to molecular polarity, flexibility, metabolic stability, and protein-binding capacity. Hierarchical clustering (Fig. 2, right panel) confirmed the existence of three robust tracer groups, each characterized by a specific pharmacological profile.

The first cluster involves TcDTPA, TcDIS, TcMAG, TcMEB, TcMED, TcDMSA, and TcECD. These tracers demonstrated balanced pharmacokinetic and interaction profiles, characterized by moderate to high polarity, generally favorable hepatic microsomal stability, and intermediate levels of protein binding, primarily to albumin. Their ADMET features support suitability for renal, hepatobiliary, and soft tissue imaging, offering flexibility in both administration protocols and imaging time windows. In turn, cluster 2 includes TcSES and TcTET, which were distinguished by low

topological polar surface area, high lipophilicity, minimal protein interaction, and rapid predicted systemic clearance. These properties reflect their optimization for myocardial perfusion imaging, where fast tracer redistribution and early acquisition are essential for diagnostic accuracy. Their distinct separation in PCA space further reinforces the pharmacological coherence of this cluster and its alignment with established clinical applications. Finally, cluster 3 contains only TcHYN, which was markedly separated from the rest in both PCA and hierarchical clustering analyses. This compound exhibited the highest polarity, the greatest number of hydrogen bond donors and acceptors, extensive conformational flexibility, and strong multivalent protein-binding potential. While these characteristics suggest utility for targeted or long-circulating applications, they also raise concerns regarding non-specific interactions and off-target effects. As such, TcHYN represents a structurally and functionally distinct tracer that warrants further experimental validation *in vivo* before broader application.

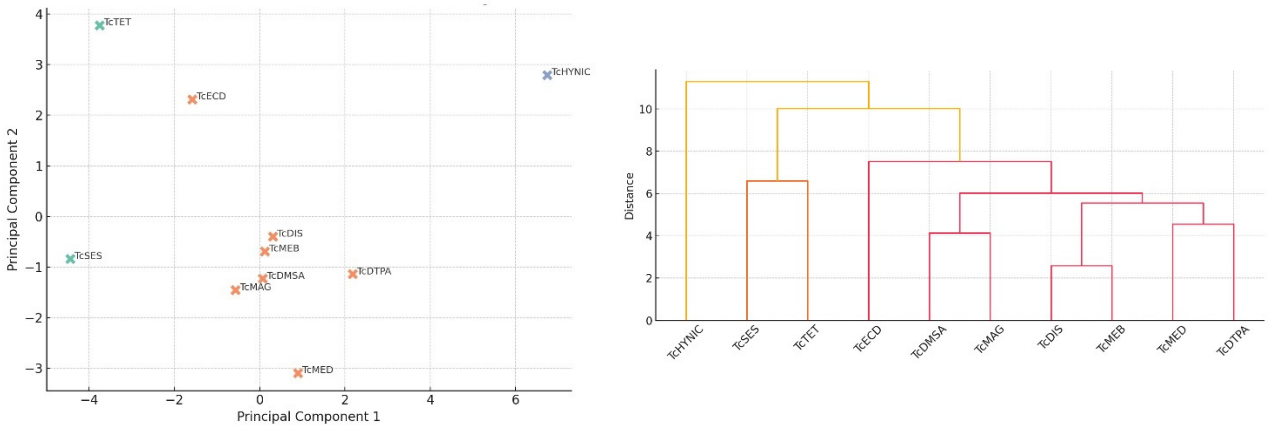

Figure 2. Cluster analysis of TCC. Left panel represents Principal Component Analysis (PCA) biplot showing tracer distribution in the space of the first two principal components. Right panel shows the dendrogram of hierarchical clustering using Ward linkage and Euclidean distance.

The integrated analysis of physicochemical descriptors, ADMET properties, and protein-binding profiles presented in this study yields several design rules for the rational development of ^{99m}Tc-labeled radiopharmaceuticals. First, polarity and permeability must be carefully matched to the intended imaging kinetics. Tracers characterized by low topological polar surface area and limited hydrogen bonding potential, such as TcSES and TcTET, demonstrate rapid systemic clearance and minimal protein binding, which make them particularly suitable for perfusion imaging or early-phase dynamic acquisitions. In contrast, compounds with moderate to high polarity, exemplified by TcDTPA and TcDIS, display extended plasma residence times and are better suited for delayed-phase protocols, including renal or hepatobiliary imaging. Another key parameter influencing *in vivo* performance is the degree of albumin interaction. Incorporation of chemical motifs that promote reversible albumin binding, such as hydrophilic chelators or carboxylate groups, can enhance plasma half-life and systemic stability. This strategy is advantageous when sustained blood pool activity is desirable; however, excessive or non-specific binding may increase background signal or delay tissue clearance, thereby complicating image interpretation in protocols that rely on rapid kinetics. Moreover, our data underscores the importance of limiting molecular flexibility and avoiding extreme polarity unless such features are deliberately employed for targeted delivery to plasma protein-rich compartments. Tracers like TcHYN, with high polar surface area and a large number of rotatable bonds, exhibit promiscuous binding across multiple protein classes, including transport and regulatory proteins. While such interactions can be beneficial in specialized contexts, they may also lead to off-target accumulation or biological interference, particularly in metabolically compromised individuals. The results outlined here also demonstrates that strong and selective binding to functional proteins, such as insulin, must be carefully evaluated *in silico* during early design stages. Although the docking-predicted affinities observed here are unlikely to disrupt hormonal function at diagnostic doses, repeated exposure or application in sensitive patient populations could present a non-negligible safety concern.

CONCLUSIONS

Taken together, the results of the present study revealed that the pharmacokinetics and protein interaction profiles of TCC are strongly influenced by their physicochemical properties. It was shown that tracers with low polarity and weak protein binding, such as TcSES and TcTET, are well suited for dynamic imaging due to their rapid clearance. In contrast, compounds like TcDTPA and TcDIS exhibited strong albumin binding and extended circulation, supporting their use in delayed-phase protocols. The analysis also identified TcHYN as a structurally distinct radiotracer with broad, high-affinity protein interactions, suggesting a higher risk of off-target effects. Multivariate classification further demonstrated that tracers could be grouped into functionally meaningful clusters, reflecting shared ADMET and binding characteristics. Overall, the findings suggest that integrated ADMET profiling and docking can provide a predictive framework for the rational design and optimization of technetium-based radiotracers.

Acknowledgements
This work was supported by the Ministry of Education and Science of Ukraine (the project № Д3/174-2025).

ORCID
Valeriya Trusova, https://orcid.org/0000-0002-7087-071X; **Uliana Malovytsia,** https://orcid.org/0000-0002-7677-0779
Galyna Gorbenko, http://orcid.org/0000-0002-0954-5053; **Pylyp Kuznietsov,** http://orcid.org/0000-0001-8477-1395
Ivan Yakymenko, http://orcid.org/0000-0001-8477-1395

REFERENCES

[1] N. Ahmed, and M. Zia, "Diagnostic modalities and radiopharmaceuticals with particular importance of technetium-99m (^{99m}Tc)," Chin. J. Acad. Radiol. **6**, 143 (2023). https://doi.org/10.1007/s42058-023-00128-7
[2] Y. Arano, "Recent advances in ^{99m}Tc radiopharmaceuticals," Ann. Nucl. Med. **16**, 79 (2002). https://doi.org/10.1007/BF02993710
[3] G. Xiong, Z. Wu, and J. Yi, "ADMETlab 2.0: an integrated online platform for accurate and comprehensive predictions of ADMET properties," Nucleic Acids Res. **49**, W5 (2021). https://doi.org/10.1093/nar/gkab255
[4] Y. Yan, H. Tao, J. He, and S. Huang, "The HDOCK server for integrated protein–protein docking," Nature Protocols, **15**, 1829 (2020). https://doi.org/10.1038/s41596-020-0312-x
[5] A. Alkandari, Y. Alsayed, and A. El-Hanbaly, "Enhanced efficacy of radiopharmaceuticals when using technetium-99m-labeled liposomal agents: synthesis and pharmacokinetic properties," Biomedicines, **10**, 2994 (2022). https://doi.org/10.3390/biomedicines10112994
[6] S. Rathmann, Z. Ahmad, S. Slikboer, H. Bilton, D. Snider, and J. Valliant, "The radiopharmaceutical chemistry of technetium-99m," in: *Radiopharmaceutical Chemistry*, edited by J. Lewis, A. Windhorst, and B. Zeglis, (Springer, Cham., 2019). http://dx.doi.org/10.1007/978-3-319-98947-1_18
[7] B. Lee, J. Yeh, N. Chiu, G. Liu, H. Yu, M. Wang, and L. Shen, "Evaluation of Tc-99m (V) DMSA binding to human plasma proteins," Kaohsiung J. Med. Sci. **24**, 1 (2008). http://dx.doi.org/10.1016/S1607-551X(08)70066-4
[8] L. Shattuck, D. Eshima, A. Taylor, *et al*., "Evaluation of the hepatobiliary excretion of technetium-99m-MAG3 and reconstitution factors affecting radiochemical purity," J. Nucl. Med. **35**, 349 (1994). https://doi.org/10.29011/2577-2201.100088
[9] A. Mori, Y. Saito, and K. Nakamura, "Microcalcification and ^{99m}Tc-pyrophosphate uptake without increased bone metabolism in cardiac tissue from patients with transthyretin cardiac amyloidosis," Int. J. Mol. Sci. **24**, 1921 (2023). https://doi.org/10.3390/ijms24031921
[10] J. Smith, and J. Pfaendtner, "Elucidating the molecular interactions between uremic toxins and the Sudlow II binding site of human serum albumin," J. Phys. Chem. B, **14**, 3922 (2020). https://doi.org/10.1021/acs.jpcb.0c02015

КОМП'ЮТЕРНЕ МОДЕЛЮВАННЯ РАДІОФАРМПРЕПАРАТІВ ТЕХНЕЦІЮ-99М: ОЦІНКА ADMET-ВЛАСТИВОСТЕЙ ТА ВЗАЄМОДІЇ З БІЛКАМИ

В. Трусова[a], У. Маловиця[a], П. Кузнєцов[b], І. Якименко[b], Г. Горбенко[a]
[a]Кафедра медичної фізики та біомедичних нанотехнологій, Харківський національний університет імені В.Н. Каразіна м. Свободи 4, Харків, 61022, Україна
[b]Кафедра фізики ядра та високих енергій імені О.І. Ахієзера, Харківський національний університет імені В.Н. Каразіна м. Свободи 4, Харків, 61022, Україна

Раціональний дизайн радіофармацевтичних препаратів на основі технецію-99m (^{99m}Tc) вимагає глибокого розуміння того, як фізико-хімічні властивості впливають на поведінку сполук *in vivo* та їхні біомолекулярні взаємодії. У даному дослідженні застосовано інтегроване комп'ютерне моделювання для характеристики десяти клінічно релевантних радіофармпрепаратів на основі технецію. Дослідження включало оцінювання ADMET-параметрів, молекулярний докінг з функціональними білками (альбуміном, інсуліном і лізоцимом), а також багатовимірний статистичний аналіз. Отримані результати показали, що полярність, здатність до утворення водневих зв'язків та молекулярна гнучкість суттєво впливають як на фармакокінетичні властивості, так і на профілі зв'язування з білками. Трейсери типу TcSES і TcTET, які характеризуються низькою топологічною полярною поверхнею та мінімальною спорідненістю до білків, продемонстрували швидке виведення з організму та виявилися придатними для динамічних протоколів візуалізації. Натомість, сполуки TcDTPA і TcDIS мали високу спорідненість до альбуміну та стабільність до продуктів метаболізму, що робить їх перспективними для візуалізації у відтерміновані фази. TcHYN, що має унікальну структуру, характеризується надмірною полярністю із широким спектром білкових взаємодій високої афінності. Аналіз головних компонент і ієрархічна кластеризація дозволили класифікувати радіофармпрепарати на функціонально відмінні групи, що підкреслює структурно-залежні закономірності дизайну. Сукупність отриманих результатів свідчать про те, що поєднання ADMET-прогнозування та молекулярного докінгу формує релевантну стратегію передклінічного скринінгу та сприяє розробці більш безпечних і таргетованих ^{99m}Tc-радіофармацевтичних препаратів.

Ключові слова: *радіофармпрепарати на основі технецію; людський сироватковий альбумін; лізоцим; інсулін; молекулярний докінг; ОФЕКТ візуалізація*